論文 / 著書情報
Article / Book Information

Title(English)	Nusselt Number Correlations for Microchannel Hot Water Supplier with S-Shaped Fins
Authors(English)	Nobuyoshi Tsuzuki, Motoaki Utamura
Citation(English)	6th Japan Korea Symposium on Nuclear Thermal Hydraulics and Safety (NTHAS6), paper No.N6P1151,
発行日 / Pub. date	2008, 11

NUSSELT NUMBER CORRELATIONS FOR MICROCHANNEL HOT WATER SUPPLIER WITH S-SHAPED FINS

Motoaki Utamura[1*], Nobuyoshi Tsuzuki[1]

[1] Research Laboratory for Nuclear Reactors

Tokyo Institute of Technology,

2-12-1 O-okayama, Meguro-ku, Tokyo, 152-8550 Japan

tel:+81357343293

fax:+81357342959

E mail: utamura@rccre.titech.ac.jp

ABSTRACT

Nusselt number correlations for microchannel heat exchanger (MCHE) with S-shaped fins are obtained by numerical experiments using 3D-CFD code and validated by experiments. Refrigerant considered here is carbon dioxide in supercritical state and assumes to operate around the pseudo-critical point. The fluid inlet temperature is defined as 2°C lower or higher than wall temperature for cold or hot side simulations, respectively. The small temperature difference is useful in reducing data because thermal-hydraulic properties can be assumed as constant for the fluid which experiences radical property change along the flow passage of the heat exchanger, e.g. when the fluid passes near pseudo-critical point. Calculations with 20 different temperature points in total are executed and those results are gathered into Nusselt number correlations for each side. The geometry size is almost 0.42% of the whole heat exchanger size. Method to calculate heat transfer performance from the correlations is also found. The heat transfer performance obtained from the correlations is compared with that of another numerical result which is reduced from large geometry and integration. They agree within 3% error and the accuracy of calculation method is confirmed. Experimental results with MCHE also verify the correlations.

1. INTRODUCTION

High performance heat exchanger is a critical component for industrial facilities with waste heat recovery in the vicinity of pseudo-critical points. A newly developed heat exchanger, named MCHE (which derives from 'Microchannel heat exchanger.' See Fig. 1), showed good heat transfer performance. (Tsuzuki, 2007) The flow channel of MCHE is created by chemical etching on metal plates and the plates are gathered to make one heat exchanger with diffusion bonding. Typical hydraulic diameter is sub-millimeter. The small hydraulic diameter increases heat transfer area and gives better heat transfer performance. The drawback of small diameter is high pressure drop. To reduce the pressure drop, new flow channel configuration named as S-shaped fin configuration has been developed. (see Fig. 2) Three dimensional computational fluid dynamics (3D-CFD) revealed that the pressure drop of S-shaped fin configuration is calculated 7 times less than that of conventional zigzag configuration.

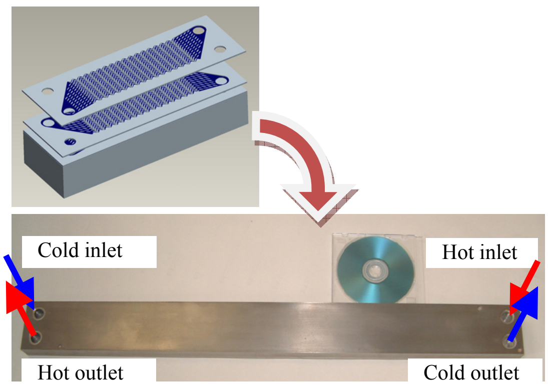

Fig. 1. Microchannel heat exchanger (MCHE).

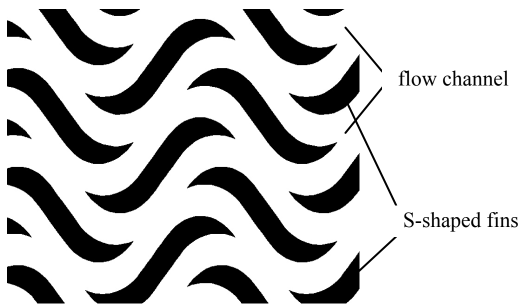

Fig. 2. S-shaped fin configuration.

In a heat exchanger, temperature and pressure of fluid varies along its flow channels. In the case of a residential heat pump system which uses supercritical carbon dioxide (CO_2). CO_2 temperature changes from over 100°C at inlet to lower than 30°C at outlet. Corresponding CO_2 pressure is 9-12 MPa, and the critical point of CO_2 is 7.4 MPa, 31°C. Hence, CO_2 in the heat exchanger of the heat pump system passes the pseudo-critical point. Figure 3 shows specific heat of CO_2 around the critical temperature. Not only specific heat but all other fluid properties changes rapidly around the pseudo-critical point.

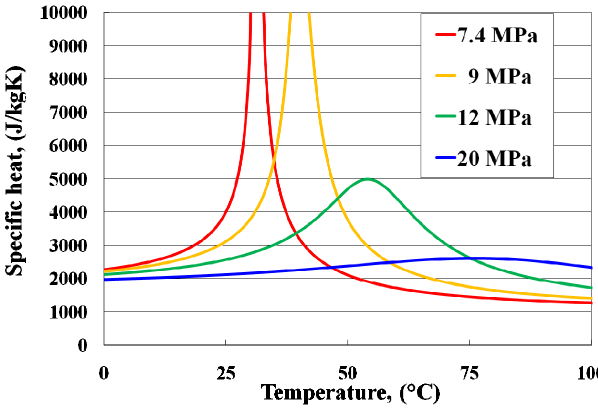

Fig. 3. Specific heat around pseudo-critical point against temperature.

The rapid change of fluid properties exerts a severe influence on the CFD calculation. If the meshes are coarse, the accuracy of calculation gets worse. While the meshes are refined enough, the mesh number may increase. The mesh number is limited by the amount of computer resources. Hence, we cannot refine the mesh enough if the computer resource is not enough. Another way to avoid radical property change inside the heat exchanger is to reduce the temperature difference between inlet and outlet. When the temperature difference is small enough, the fluid property change can be supposed as constant. However, small temperature difference means that only a part of a heat exchanger can be simulated.

In this study, CFD simulation calculations with small temperature difference were examined. The condition of the residential heat pump system was considered as reference when the inlet conditions of fluid were determined. As described above, CO_2 in the heat exchanger passes pseudo-critical point. However, the temperature difference of fluid was small, 2°C. Thus, rapid property change of fluid will be avoided. From the calculations changing inlet temperature and flow rate, Nusselt number correlations for each cold and hot side are obtained. A new method to evaluate the heat transfer performance of whole heat exchanger from these empirical correlations was also proposed. The method through the new correlations was verified by comparison with another simulation result with large geometry and experimental results using a test piece of the MCHE.

2. MCHE and S-shaped fin configuration

MCHE, which derives from 'Microchannel Heat Exchanger', is defined as a heat exchanger composed of metal plates which have milled flow channels by chemical etching. Those plates are gathered to produce one block using diffusion bonding technology. Hydraulic diameter of the channel created using chemical etching is the order of one millimeter. The small hydraulic diameter contributes to increase heat transfer area and heat transfer performance of MCHE, and it also works to reduce the stress force in MCHE. Diffusion bonding can produce MCHE without strength reduction of the material. Thus, MCHE has high heat transfer performance and high anti-pressure performance.

At the same time, small hydraulic diameter gives high pressure drop. Pressure drop is one of the important factors for heat exchanger performance. To reduce the pressure drop of MCHE, the new flow configuration named S-shaped fin configuration (given above in Fig. 2) has been proposed. Numerical study by CFD code was examined and it was found that pressure drop of S-shaped fin configuration is about one seventh compared with conventional zigzag configuration while the heat transfer rate of S-shaped fin configuration is almost same as zigzag configuration. (Tsuzuki, 2007)

Experimental verification for the advantages of the S-shaped fin configuration was examined as a recuperator of a supercritical CO_2 gas turbine cycle (Nikitin, 2006) and as a hot water supplier of a residential CO_2 heat pump system (T. L. Ngo, 2006) The difference of heat transfer performance was 5-10%, thus, a numerical evaluation of MCHE by CFD code was confirmed to have enough accuracy for designing.

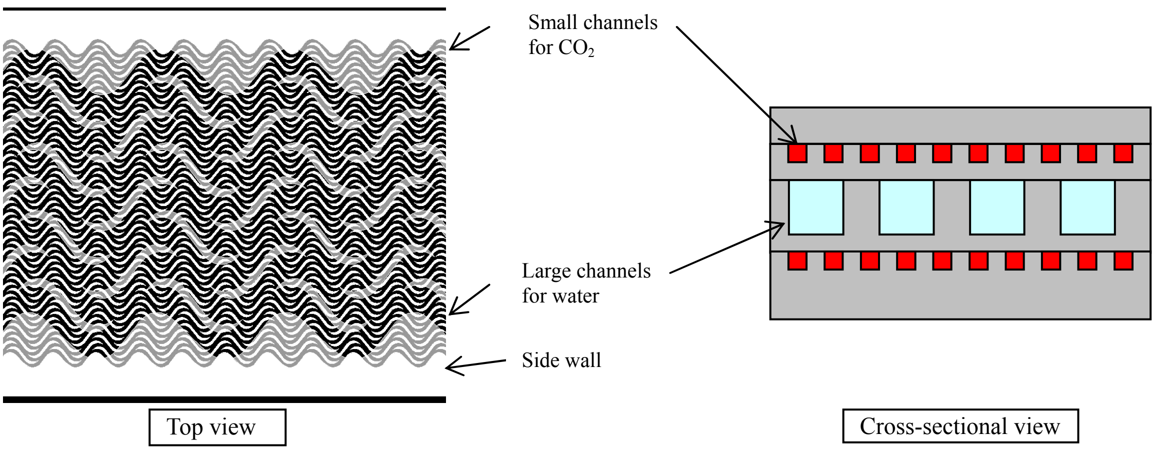

Fig. 4. Top view and cross-sectional view of MCHE hot water supplier.

3. Calculation Model

The geometry of the MCHE in this study is designed for a residential heat pump system (T. L. Ngo, 2006) The heat exchanger is made of copper and composed of cold water channels and hot CO_2 channels. The top view and cross-sectional view is given in Fig 4. The whole heat exchanger size is 1240×68×4.75 (mm).

To attain accurate empirical correlations using small temperature difference, the simulation calculations were examined for each hot and cold side separately.

The cold (water) side includes large S-shaped fins in its flow channels. The calculation model of cold side is shown in Fig. 5. The model size is 90.78×12.37×1.35 (mm), that is almost 0.42% of the whole heat exchanger. About boundary conditions, periodic condition was applied to the both side walls. The bottom plane is symmetrical plane. And the temperature of top wall was 2°C higher than the fluid inlet temperature all the way along the channel. The inlet temperature was 278.15 K and 358.15 K, to simulate a part near the inlet and outlet of the heat exchanger. Flow rate was varied in the range of 6.04×10^{-4}-1.75×10^{-3} kg/s.

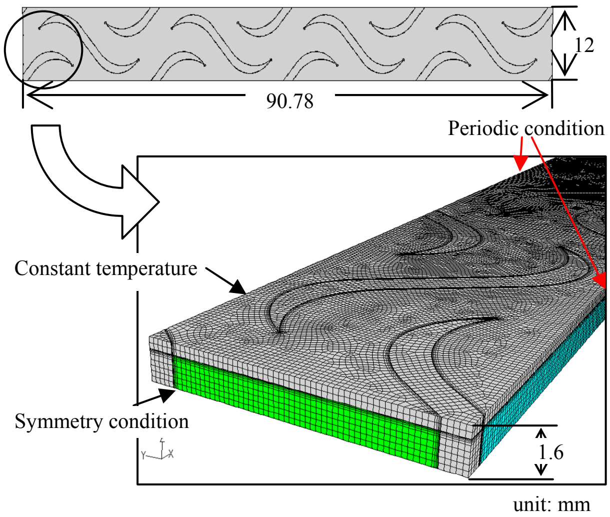

Fig. 5. Simulation geometry for water side.

The hot (CO_2) side includes small fins. The geometry size is 90.78×12×1.69 (mm), almost same as that of cold side. The both side walls are under periodic condition, and the bottom wall is under adiabatic condition. The top wall temperature was set 2°C lower than the inlet temperature of fluid along the channel. The hot side geometry is summarized in Fig. 6. Since CO_2 passes the pseudo-critical point, inlet temperature of 393.15, 293.15 and 327.15 were used to simulate a part near the inlet, outlet and where the pseudo-critical point is realized, respectively. Flow rate was changed 9.26×10^{-4}-2.47×10^{-3} kg/s. The both fluid conditions are summarized in Table 1.

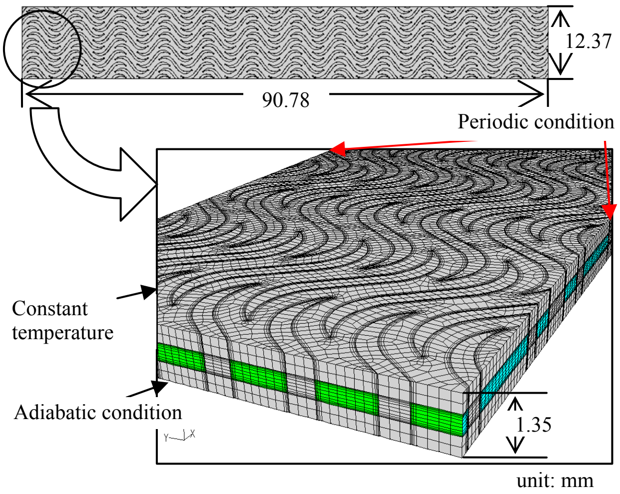

Fig. 6. Simulation geometry for CO_2 side.

Simulation calculations were carried out using 3D-CFD code, FLUENT. (ANSYS Inc., 2007) Governing equations considered are the continuity, momentum and energy equations. Turbulence was taken into account by the ReNormalization Group (RNG) k-ε model and wall function. All equations were solved using second-order upwind discretization for convection. The Semi Implicit Method Pressure Linked Equation (SIMPLE) algorithm was used to resolve coupling of velocity and pressure.

Thermodynamic properties of CO_2 (density, viscosity, specific heat, and thermal conductivity) were calculated using PROPATH, a database for thermo-physical properties of fluids. (Ito *et al.*, 1990) The fluid is assumed to be in local equilibrium for thermodynamic and transport properties. Free convection, viscous dissipation, and compressive work are neglected in this simulation. The property values of copper initially given in FLUENT are used as metal plate properties.

Mesh size, as generated by GAMBIT, was varied from the wall to the central flow region. At the vicinity of wall surfaces, the minimum mesh size was 0.015 mm. Such fine mesh units were allocated into five rows from the fin wall surfaces. The mesh size was about 0.2 mm for regions that were distant from wall surfaces.

The numbers of meshes are almost 1.4 million for hot side simulation, and 600 thousand for cold side simulation. This

Table 1. Inlet condition of working fluid for single side simulations.

	Water, near inlet	*near outlet*	*CO_2, near inlet*	*near pseudo-CP*	*near outlet*
Inlet temperature of fluid, T_{in} [K]	278.15	358.15	393.15	327.15	293.15
Temperature of top wall, T_{wall} [K]	280.15	360.15	391.15	325.15	291.15
Mass flow rate, [$\times10^{-3}$ kg/s]	0.604, 0.931, 1.18, 1.75		0.926, 1.44, 1.96, 2.47		
Inlet pressure, [MPa]	0.25		12		

simulation used a calculating time of about 12 hours with 4 AMD Opteron ™ CPUs for 3000 iterations.

3. Results

Table 2 shows the results of simulation calculations for cold (water) side. Condition #1-4 are simulating near the water inlet of the heat exchanger, and #5-8 are near the outlet. Hot (CO_2) side results are shown in Table 3. For hot side, #1-4 are the results near the inlet of CO_2, #5-8 are near the outlet and #9-12 are near the pseudo-critical point at the pressure.

Table 2. Calculation results and Reynolds, Prandtl, Nusselt numbers of each simulation for cold (water) side.

#		1	2	3	4	5	6	7	8
Inlet temperature, T_{in}	[K]	278.15	278.15	278.15	278.15	358.15	358.15	358.15	358.15
Outlet temperature, T_{out}	[K]	279.32	279.19	279.11	279.00	359.64	359.52	359.46	359.35
Temperature of wall, T_{wall}	[K]	280.15	280.15	280.15	280.15	360.15	360.15	360.15	360.15
Mass flow rate, W	[$\times10^{-3}$ kg/s]	0.604	0.931	1.177	1.750	0.604	0.931	1.177	1.750
Heat load, Q	[W]	2.97	4.05	4.73	6.22	3.78	5.38	6.48	8.85
Reynolds number, Re	[-]	109.7	168.8	213.1	316.4	495.2	762.7	963.9	1432
Prandtl number, Pr	[-]	10.95	10.97	10.98	11.00	2.075	2.077	2.077	2.079
Nusselt number, Nu	[-]	9.887	12.67	14.30	17.97	13.17	17.21	19.97	25.63

Table 3. Calculation results and Reynolds, Prandtl, Nusselt numbers of each simulation for hot (CO_2) side.

#		1	2	3	4	5	6
Inlet temperature, T_{in}	[K]	393.15	393.15	393.15	393.15	293.15	293.15
Outlet temperature, T_{out}	[K]	391.16	391.18	391.20	391.21	291.16	291.18
Temperature of wall, T_{wall}	[K]	391.15	391.15	391.15	391.15	291.15	291.15
Mass flow rate, W	[$\times10^{-3}$ kg/s]	0.926	1.440	1.955	2.469	0.926	1.440
Heat load, Q	[W]	2.76	4.26	5.73	7.19	4.44	6.87
Reynolds number, Re	[-]	5569	8662	11759	14851	1505	2341
Prandtl number, Pr	[-]	1.037	1.037	1.037	1.037	2.070	2.070
Nusselt number, Nu	[-]	49.72	61.41	73.36	87.92	26.84	34.59

	7	8	9	10	11	12
T_{in}	293.15	293.15	327.15	327.15	327.15	327.15
T_{out}	291.19	291.20	325.23	325.29	325.34	325.38
T_{wall}	291.15	291.15	325.15	325.15	325.15	325.15
W	1.955	2.469	0.926	1.440	1.955	2.469
Q	9.26	11.6	8.19	12.4	16.4	20.2
Re	3178	4014	3327	5180	7038	8895
Pr	2.070	2.070	2.884	2.884	2.884	2.884
Nu	41.92	49.81	50.24	64.87	77.93	90.55

Nusselt numbers of each result were calculated as follows.

Heat load is obtain as Eq. (1),

$$Q = [H(T_{in}) - H(T_{out})] \times W \tag{1}$$

where $H(T)$ is specific enthalpy at temperature, T. T_{in} and T_{out} are inlet and outlet temperature, respectively. W is the flow rate.

Logarithmic mean temperature difference, ΔT_{LMTD}, may be defined where physical properties are assumed as constant using wall temperature, T_{wall}, as follows,

$$\Delta T_{LMTD} = \frac{(T_{wall} - T_{in}) - (T_{wall} - T_{out})}{\log[(T_{wall} - T_{in})/(T_{wall} - T_{out})]} \tag{2}$$

If physical properties are not constant, another method to calculate the temperature difference should be applied. (Utamura, 2008) From the method, the temperature difference is defined without the assumption of constant specific heat. Thus, the generalized temperature difference, ΔT_{GMTD}, can be an accurate index however the physical properties are changed. For the cases shown in Table 2 and 3, ΔT_{LMTD} and ΔT_{GMTD} were compared and the maximum difference was 0.010 K for the case number 5 of Table 3 (2.7%). The difference is enough small, and it is confirmed that ΔT_{LMTD} has enough accuracy under the small temperature difference condition.

From Q and ΔT_{LMTD}, heat transfer coefficient, h, is calculated,

$$h = \frac{Q}{\Delta T_{LMTD} \cdot A} \tag{3}$$

where A is heat transfer area. In this study, heat transfer area is defined as the sum of all the wet area, including side walls in addition to top and bottom wall.

Thus, Nusselt number, Nu, is calculated from h as Eq. (4),

$$Nu = \frac{h \cdot D_h}{\lambda} \tag{4}$$

where λ is thermal conductivity of fluid, and D_h is hydraulic diameter of the channel defined as (4V/A) with V the volume of the fluid in the channel.

The calculated heat load and Nusselt number were also summarized in Table 2 and 3.

4. Discussions

4.1 Flow in S-shaped fin configuration: laminar or turbulent

Reynolds number in S-shaped fin configuration is usually about $1500 < Re_{CO2} < 15000$ for CO_2, and $100 < Re_{H2O} < 500$ for water. While Reynolds number at CO_2 side is large enough to regard as turbulent flow, Reynolds number at water side is relatively small. However, the S-shaped fin configuration is composed of many discontinuous fins located in the flow channel and flow stream is separated around the channel. Thus, the water flow in S-shaped fin configuration is not fully developed laminar flow.

For fully developed laminar flow, Nusselt number correlation of circular tube is given as, (Katto, 1964)

$$Nu_x = \frac{h_x D_h}{\lambda} = 1.063(RePr\frac{D_h}{x})^{1/3} \tag{5}$$

From Eq. (5), $(Nu/Pr^{1/3})$ may depend on $Re^{1/3}$ when the flow is fully developed laminar flow.

When the flow is turbulent, Utamura reported Nusselt number correlation in MCHE for both fluids water and CO_2, (Utamura, 2007)

$$Nu = 0.0473\ Re^{0.8}\ Pr^{0.6} \tag{6}$$

Thus, in turbulent flow, $(Nu/Pr^{0.6})$ may depend on $Re^{0.8}$.

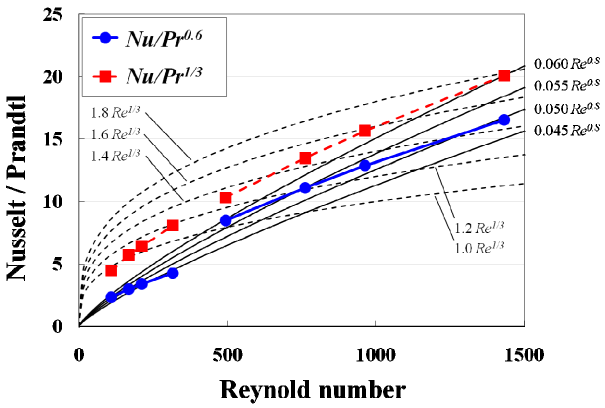

Fig. 7. Nusselt number over Prandtl number as a function of Reynolds number.

Figure 7 shows both $(Nu/Pr^{0.6})$ and $(Nu/Pr^{1/3})$ against Reynolds number. The referential lines of $Re^{0.8}$ and $Re^{1/3}$ are also shown by solid line and broken line. Judging from Fig. 7, the flow of water in S-shaped fin configuration is rather turbulent than laminar though Reynolds number of water is small.

4.2 New Nusselt number Correlations

A literature survey for heat transfer of supercritical fluid was examined. (Pioro, 2004, 2007) In these surveys, many empirical correlations were listed and compared with experimental results. Pioro concluded that three correlations, Gorban', Dyadyakin and Popov, and Bringer and Smith showed results that are close to the experimental data. The two of three correlations, Gorban' and Bringer and Smith correlations, are expressed as the combination of polynomials of Reynolds number and Prandtl number. Thus, the Nusselt number correlations constructing in this study is expressed as follows,

$$Nu = \alpha\ Re^{\beta}\ Pr^{\gamma} \tag{7}$$

Eq. (7) can be rewritten into logarithmic form,

$$\ln Nu = \ln \alpha + \beta \ln Re + \gamma \ln Pr$$
$$= \alpha' + \beta \ln Re + \gamma \ln Pr \tag{8}$$

where $\alpha' \equiv \ln \alpha$ (9)

Using the Nusselt number calculated from each calculation result, Nu_i, the square difference between Nu and Nu_i, ϕ, is defined as follows,

$$\phi = \sum_{i=1}^{N} (\ln Nu - \ln Nu_i)^2 = \sum_{i=1}^{N} (\ln \frac{Nu}{Nu_i})^2 \tag{10}$$

where N is total number of calculation results.

The square difference ϕ' is minimized when

$$\frac{\partial \phi}{\partial \alpha'} = \frac{\partial \phi}{\partial \beta} = \frac{\partial \phi}{\partial \gamma} = 0 \tag{11}$$

Hence, the optimal Nusselt number correlation is obtained using Eq. (11). $\frac{\partial \phi}{\partial \alpha'}$, $\frac{\partial \phi}{\partial \beta}$, $\frac{\partial \phi}{\partial \gamma}$ are given by Eq. (10),

$$\frac{\partial \phi}{\partial \alpha'} = \sum_{i=1}^{N} 2(\ln Nu - \ln Nu_i) \cdot 1 = 0 \tag{12}$$

$$\frac{\partial \phi}{\partial \beta} = \sum_{i=1}^{N} 2(\ln Nu - \ln Nu_i) \cdot \ln Re_i = 0 \tag{13}$$

$$\frac{\partial \phi}{\partial \gamma} = \sum_{i=1}^{N} 2(\ln Nu - \ln Nu_i) \cdot \ln Pr_i = 0 \tag{14}$$

Eq. (8) replaces $\ln Nu$ in Eq. (12)-(14) as,

$$\sum_{i=1}^{N} (\alpha' + \beta \ln Re_i + \gamma \ln Pr_i - \ln Nu_i) = 0 \tag{15}$$

$$\sum_{i=1}^{N} \{(\alpha' + \beta \ln Re_i + \gamma \ln Pr_i - \ln Nu_i) \cdot \ln Re_i\} = 0 \tag{16}$$

$$\sum_{i=1}^{N} \{(\alpha' + \beta \ln Re_i + \gamma \ln Pr_i - \ln Nu_i) \cdot \ln Pr_i\} = 0 \tag{17}$$

Thus,

$$\begin{pmatrix} \sum 1 & \sum \ln Re_i & \sum \ln Pr_i \\ \sum \ln Re_i & \sum (\ln Re_i)^2 & \sum (\ln Re_i \ln Pr_i) \\ \sum \ln Pr_i & \sum (\ln Re_i \ln Pr_i) & \sum (\ln Pr_i)^2 \end{pmatrix} \begin{pmatrix} \alpha' \\ \beta \\ \gamma \end{pmatrix} = \begin{pmatrix} \sum \ln Nu_i \\ \sum (\ln Nu_i \cdot \ln Re_i) \\ \sum (\ln Nu_i \cdot \ln Pr_i) \end{pmatrix} \tag{18}$$

Equation (18) gives α, β, γ with Eq. (9), and finally following Nusselt number correlations were obtained using simulation results for each side individually.

$$\begin{cases} \text{Cold side (Water side):} \\ \qquad Nu = 0.262\ Re^{0.594}\ Pr^{0.346} \\ \text{Hot side } (CO_2 \text{ side}): \\ \qquad Nu = 0.229\ Re^{0.617}\ Pr^{0.345} \end{cases} \tag{19}$$

Newly obtained correlations Eq. (19) were confirmed by calculating Nusselt numbers using Reynolds numbers and Prandtl numbers given in Table 2 and 3. The calculation results of Eq. (19), Nu_{corr}, were plotted against Nusselt numbers obtained for each calculation through Eq. (4), Nu_{CFD}, in Fig. 8. Nu_{corr} shows good agreement with Nu_{CFD}, the deviation of the correlations are σ = 1.31% for water side and σ = 1.94% for CO_2 side. Nusselt numbers calculated from ref. (Katto, 1964), Utamura (Utamura, 2007) and Dittus-Boelter correlations were also plotted in Fig.8. It is clear that the new correlations, Eq. (19), can reproduce the Nusselt number the best among these correlations.

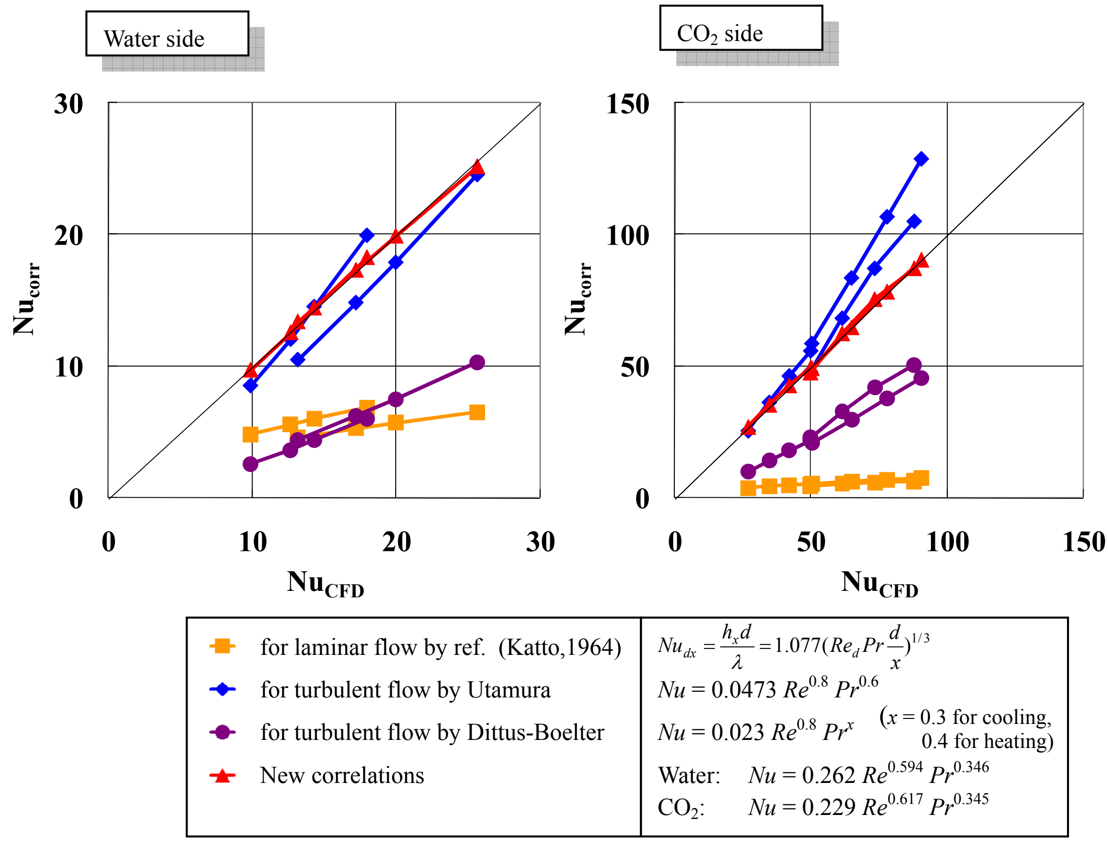

Fig. 8. Nusselt number comparison between obtained from CFD and calculated from Eq. (19).

There are many correlations for turbulent flow. Formerly, Dittus and Boelter found the famous correlation in 1930. After that, many correlations were found and recently many empirical correlations for microchannel heat exchangers were obtained.(Utamura, 2008; Pioro, 2004, 2007; Fernando, 2008) According with these correlations, the power exponent of Reynolds number usually varies around 0.8-1.2. The new correlations given as Eq. (19) have smaller power exponents of Reynolds number than others. In the flow channels of the S-shaped fin configuration, the working fluid goes smoothly and effectively throughout the channels. The flow profile is quite uniform, hence fluid velocity in S-shaped fin configurations is smaller than that in other configurations. As described above, discontinuous fins of the configuration tend to make the flow turbulent. The total heat transfer performance of the S-shaped fin configuration is higher than which conventional correlations give as seen Fig. 8. Consequently, the S-shaped fin configuration may have special characteristics to increase heat transfer performance and Reynolds number effect on Nusselt number correlations becomes weaker.

4.3 Heat transfer performance of the whole heat exchanger from single side correlations

The correlations Eq. (19) were applicable for only a single (cold or hot) side. To evaluate the heat transfer performance of whole heat exchanger, a new method to assemble the correlations is proposed.

The overall heat transfer coefficient, U, derives from,

$$Q = U\,A\,\Delta T \tag{20}$$

where Q: heat transfer amount, A: heat transfer area, ΔT: temperature difference between cold and hot side.

U and ΔT are independent on A. The derivative of Eq. (20) gives,

$$\frac{dQ}{dA} = U\,\Delta T \tag{21}$$

Q and ΔT are functions of temperature, and U and A are geometrical factors. Thus, Eq. (21) becomes,

$$\frac{dQ}{\Delta T} = U\,dA \tag{22}$$

$$\therefore \int \frac{dQ}{\Delta T} = \int U\,dA \tag{23}$$

The heat exchanger was divided into sections with the heat transfer amount. In this study, the number of divided sections, M, is 1000. The fluid temperature at each section was calculated from specific enthalpy at the section. The pressure assumed changing linearly from inlet to outlet because pressure drop is relatively small than inlet pressure. Other fluid properties were calculated from temperature and pressure at the section.

When Eq. (20) is applied to each section, it gives

$$U_i = \frac{Q_i}{A_i\,\Delta T_i} \tag{24}$$

where Q_i is heat transfer amount at the section, (= Q/N). Heat conductance U_iA_i (≡ C_i) is common to both fluid and overall heat transfer coefficient for a single side is calculated by C_i/A_i.

The reciprocal of U means an overall heat transfer resistance. The resistance can be considered as having the components of a cold side convection, a hot side convection and a wall conduction. The thermal resistance of copper is very small, typically of the order of 1/50 of other heat transfer resistances. Thus, the wall conduction component is neglected, giving

$$\frac{1}{U^C A^C} = \frac{1}{h^C A^C} + \frac{1}{h^H A^H}$$

$$= \frac{D_h^C}{Nu^C \cdot \lambda^C} \cdot \frac{1}{A^C} + \frac{D_h^H}{Nu^H \cdot \lambda^H} \cdot \frac{1}{A^H} \tag{25}$$

$$U^C = 1 \Bigg/ \left(\frac{D_h^H}{Nu^H \cdot \lambda^H} \cdot \frac{A^C}{A^H} + \frac{D_h^C}{Nu^C \cdot \lambda^C} \right) \tag{26}$$

Since (A^C/A^H) can be considered as constant over the whole heat exchanger, U_i^C is obtained from Eq. (19) and Eq. (26) regardless of the values of A_i^C and A_i^H. The heat transfer area of cold side at the section, A_i^C, is calculated by given U_i^C,

$$A_i^C = \frac{Q_i}{U_i^C \cdot \Delta T_i} \tag{27}$$

Mean overall heat transfer coefficient of cold side averaged over the whole heat exchanger obtained from the correlations, U^C_{corr}, is defined through Eq. (23) as follows,

$$U^C_{corr} \equiv \frac{\int U^C \, dA}{A^C} = \frac{\sum \left(U_i^C \cdot A_i^C \right)}{\sum A_i^C} \tag{28}$$

Mean temperature difference, $\overline{\Delta T}$, is defined as well,

$$\overline{\Delta T} \equiv \frac{Q}{\int \frac{dQ}{\Delta T}} = \frac{M}{\sum_{i=1}^{M} \frac{1}{\Delta T_i}} \tag{29}$$

4.4 Verification of the whole heat transfer performance obtained from new Nusselt correlations

Another simulation calculations for the heat exchanger were already examined. (T. L. Ngo, 2007) The heat exchanger was divided into 10 sections with its heat transfer amount. Overall heat transfer coefficients for each section were calculated using logarithmic mean temperature difference and overall heat transfer coefficient of the whole heat exchanger was obtained by integrating the polynomial fitting function of each overall heat transfer coefficient. In Ngo's study, all the heat exchanger parts were simulated even though the lengths for simulation are not correct. Thus, simulation result of Lam is more accurate calculation with more computer resources than that of this study. The inlet condition of the calculation is summarized in Table 4. From the result, the overall heat transfer coefficient of the whole heat exchanger, U^C_{whole}, was calculated as 3037 W/m^{2}K. Using Eq. (19) and Eq. (28), the heat transfer performance from the new correlations with the same condition was calculated as, U^C_{corr} = 3114 W/m^{2}K. The difference was within 3%. Therefore, it is confirmed that the new Nusselt number correlations, Eq. (19), and the assembling method given as Eq. (28) can reproduce the heat transfer performance of the whole heat exchanger with less computer resources.

Table 4. Inlet and outlet condition of the numerical result with whole geometry of the heat exchanger.

	hot side (CO_2 side)	cold side (water side)
Inlet temp., T_{in} (°C)	118.0	7.0
Outlet temp., T_{out} (°C)	77.0	27.7
Flow rate, W (kg/hr)	57.8	48.0
Heat transfer amount (kW)	4.6	

T. L. Ngo also examined experimental studies of thermal-hydraulic performance using a test piece of the microchannel heat exchanger. For the experimental data, only total heat transfer amount and inlet/outlet temperature and pressure of the whole heat exchanger were measured.

From the inlet/outlet temperature of fluid, total transferred heat amount was calculated. Since given heat from hot side includes heat loss, received heat of cold side was considered as equivalent to the true heat transfer amount. Using the heat transfer amount, the heat exchanger could be divided into M sections as well as numerical analysis. For each section, the temperature was calculated from the specific enthalpy of the section and the pressure was calculated with the assumption that the pressure was changing linearly from inlet to outlet. Mean temperature difference, $\overline{\Delta T}$, was also calculated using Eq. (29) for experimental analysis as well. Thus, the heat transfer performance of experiment, U^C_{exp}, was calculated as following Eq. (30).

$$U^C_{\exp} = \frac{Q}{A \cdot \overline{\Delta T}} \tag{30}$$

The comparison of heat transfer performance over whole heat exchanger with experimental results, U^C_{exp}, and numerical results from Eq. (19) and Eq. (28) ,U^C_{corr}, is shown in Fig. 9. The derivation of the comparison is approximately 3.09%. From the result, following relationship of U^C_{corr} to U^C_{exp} was obtained.

$$U^C_{corr} = 1/1.0396\, U^C_{exp} \tag{31}$$

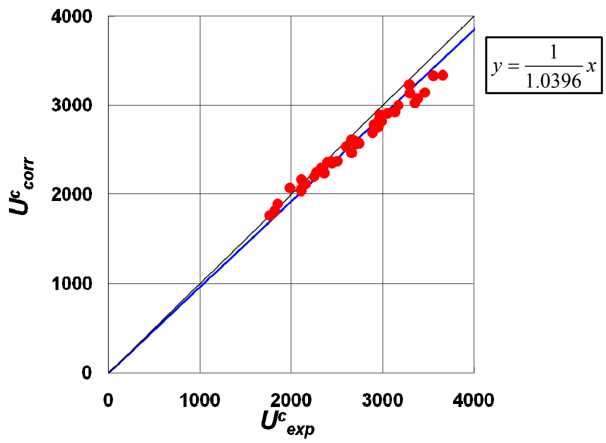

Fig. 9. Overall heat transfer coefficient comparison between U^C_{exp} and U^C_{corr}.

Numerical result of heat transfer performance was 4% smaller than the experimental result about overall heat transfer coefficient. Hence the new Nusselt number correlations can evaluate the experimental performance of the heat exchanger as well.

The actual MCHE has some roundness in its flow channel due to chemical etching. (see Fig. 10) The roundness changes the flow profile and may cause the difference of overall heat transfer coefficient. The simulation calculation was examined for the geometry shown in Fig. 11, in which the radius of roundness is 0.2 mm. When the heat transfer area of the rounded geometry is supposed as same as non-rounded one, the overall heat transfer coefficient of the rounded model is about 0.5% smaller than that of non-rounded model. The effect of roundness on heat transfer performance is small. It was concluded that the difference of heat transfer performance between experimental result and Eq. (19) was due to decreased heat transfer performance in the distributor which exists near the inlet and outlet only in the real heat exchanger. Consequently, the new correlations for each side and the method to assemble them for the evaluation of the whole heat transfer performance were successfully confirmed by the comparison with another numerical result and experimental results.

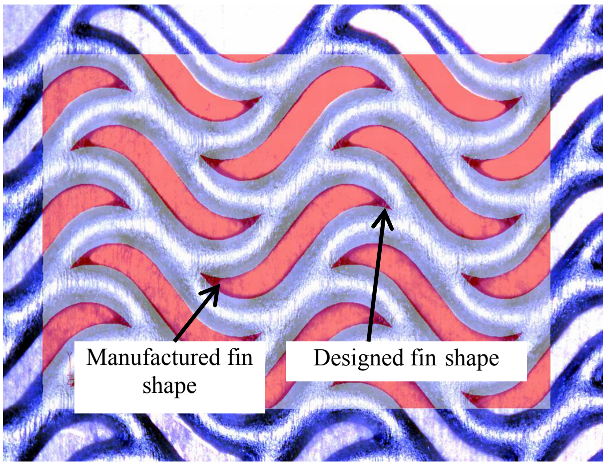

Fig.10. Roundness observed in the test piece of S-shaped fin configuration.

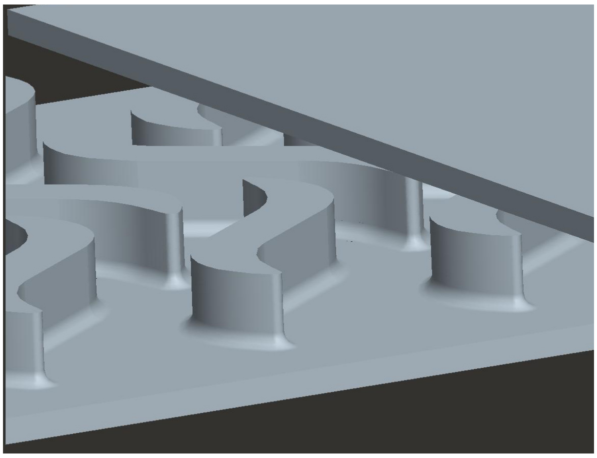

Fig. 11. Geometry of rounded model, the radius of roundness is 0.2 mm.

5. Conclusions

Nusselt number calculations for the hot water supplier of microchannel heat exchanger with S-shaped fin configuration were obtained.

$$\begin{cases} \text{Cold side (Water side):} & Nu = 0.262\, Re^{0.594}\, Pr^{0.346} \\ & (100<Re<1500,\ 2<Pr<11) \\ \text{Hot side } (CO_2 \text{ side}): & Nu = 0.229\, Re^{0.617}\, Pr^{0.345} \\ & (1500<Re<15000,\ 1<Pr<3) \end{cases}$$

The Nusselt number correlations were numerically obtained for each cold/hot side using small temperature difference between fluid inlet and wall. The simulation calculations with small temperature difference reproduced gave more accurate prediction when the fluid properties vary rapidly along the flow channels.

A method to assemble these correlations to evaluate the heat transfer performance of the whole heat exchanger was also proposed. The method succeeded to reproduce the heat transfer performance obtained from another large-scale calculations or experimental results within 3% or 4% error, respectively. Therefore, the correlations for a single side obtained using small computational resources could evaluate the whole heat exchanger performance accurately.

NOMENCLATURE

A	heat transfer area,	[m^2]
C	heat conductance,	[W/m^2]
D_h	hydraulic diameter,	[m]
$H(T)$	enthalpy at temperature T,	[J/kg K]
h	(local) heat transfer coefficient,	[W/m^{2}K]
M	number of divided sections (= 1000)	
N	number of simulation calculations; 12 for CO_2 side, 8 for water side	
Nu	Nusselt number,	[-]
P	pressure,	[Pa]
Pr	Prandtl number,	[-]
Q	heat load,	[W]
Re	Reynolds number,	[-]
T	temperature,	[K]
U	overall heat transfer coefficient,	[W/m^{2}K]
W	mass flow rate,	[kg/s]
x	distance from inlet,	[m]

Greek

ΔT	temperature difference,	[K]
$\overline{\Delta T}$	mean temperature difference,	[K]
ΔT_{GMTD}	generalized mean temperature difference,	[K]
ΔT_{LMTD}	logarithmic mean temperature difference,	[K]
λ	thermal conductivity of fluid,	[W/m K]
ϕ	the square difference given in Eq. (10),	[-]

Superscript

C	cold side (water side)
H	hot side (CO_2 side)

Subscript

i	at the section i
in	at inlet
$wall$	at wall
x	at distance x from inlet

REFERENCES

N. Tsuzuki *et al.* (2007). “High performance printed circuit heat exchanger”, *App. Therm. Eng.*, **27**, pp. 1702-1707.

K. Nikitin et al. (2006). “Printed circuit heat exchanger thermal-hydraulic performance in supercritical CO_2 experimental loop”, *Int. J. Refrig.*, **29**, pp. 807-814.

T. L. Ngo *et al.* (2006). “New printed circuit heat exchanger with S-shaped fins for hot water supplier”, *Exp. Therm. Fluid Sci.*, **30**, pp. 811-819.

ANSYS Inc. (2007). *Fluent 6.3 User’s guide*, Fluent Inc., Lebanon, NH.

T. Ito *et al.* (1990). *PROPATH: A Program Package for Thermo-physical Properties of Fluids, Version 10.2*, Corona Publishing Co., Tokyo.

M. Utamura *et al.* (2008). “A generalized mean temperature difference method for thermal design of heat exchangers”, *Int. J. Nucl. Energy Sci. Tech.*, **4**, 1,pp. 11-31.

M.Utamura *et al.* (2007). “Empirical Correlations for Thermal-Hydraulic Characteristics of Compact Heat Exchangers with Microchannels”,NTHAS5-N001, Proc. of 5th Korea-Japan Symposium on Nuclear Thermal-Hydraulics and Safety, Nov. 2006, Jeju Korea,pp.733-740

Y. Katto (1964). *Dennetsu Gairon*, Yokensha. [in Japanese]

I. L. Pioro *et al.* (2004). “Heat transfer to supercritical fluids flowing in channels-empirical correlations(survey)”, *Nucl. Eng. Design*, **230**, pp. 69-91.

I. L. Pioro *et al.* (2007). *Heat transfer and hydraulic resistance at supercritical pressures in power engineering applications,* ASME press, New York, NY.

P. Fernando *et al.* (2008). “A minichannel aluminium tube heat exchanger – Part I: Evaluation of single-phase heat transfer coefficients by the Wilson method”, *Int. J. Refrig.*, **31**, pp. 669-680.

T. L. Ngo (2007), *Doctorial thesis at Tokyo Institute of Technology*.

Appendix 1　The accuracy of the experiments

The measurement accuracy of each sensor are listed in Table 5. Considering that the transferred heat was calculated from only cold (water) side temperature and flow rate, the total uncertainty of the experiment is calculated as 2.12%.

Table 5　Maximum uncertainties of sensors.

	Max. Uncertainty
Thermistor,	±0.5°C
Flow meter,	±2% F.S.